

Article

Improved Photocatalytic H₂ Evolution by Cobaloxime-Tethered Imidazole-Functionalized Periodic Mesoporous Organosilica

M. Ángeles Navarro , Miguel A. Martín, José Rafael Ruiz , César Jiménez-Sanchidrián, Francisco J. Romero-Salguero *  and Dolores Esquivel * 

Departamento de Química Orgánica, Instituto Químico para la Energía y el Medioambiente (IQUEMA), Facultad de Ciencias, Campus de Rabanales, Universidad de Córdoba, 14071 Córdoba, Spain

* Correspondence: qo2rosaf@uco.es (F.J.R.-S.); q12esmem@uco.es (D.E.); Tel.: +34-957-218638 (F.J.R.-S.); +34-957-211050 (D.E.)

Abstract: Molecular cobaloxime-based heterogeneous systems have attracted great interest during the last decades in light-driven hydrogen production. Here, we present a novel cobaloxime-tethered periodic mesoporous organosilica (PMO) hybrid (Im-EtPMO-Co) prepared through the immobilization of a molecular cobaloxime complex on the imidazole groups present in ethylene-bridged PMO. The successful assembly of a molecular cobaloxime catalyst via cobalt-imidazole axial ligation has been evidenced by several techniques, such as ¹³C NMR, Raman spectroscopy, ICP-MS, and XPS. The catalytic performance of Im-EtPMO-Co catalyst was essayed on the hydrogen evolution reaction (HER) under visible light in presence of a photosensitizer (Eosin Y) and an electron donor (TEOA). It showed an excellent hydrogen production of 95 mmol hydrogen at 2.5 h, which corresponded to a TON of 138. These results reflect an improved photocatalytic activity with respect to its homogenous counterpart [Co(dmgH)₂(Im)Cl] as well as a previous cobaloxime-PMO system with pyridine axial ligation to the cobaloxime complex.

Keywords: cobaloxime; periodic mesoporous organosilicas; photocatalysis; hydrogen evolution reaction; primary axial coordination



Citation: Navarro, M.Á.; Martín, M.A.; Ruiz, J.R.; Jiménez-Sanchidrián, C.; Romero-Salguero, F.J.; Esquivel, D. Improved Photocatalytic H₂ Evolution by Cobaloxime-Tethered Imidazole-Functionalized Periodic Mesoporous Organosilica. *Hydrogen* **2023**, *4*, 120–132. <https://doi.org/10.3390/hydrogen4010008>

Academic Editor: Shreya Mukherjee

Received: 5 November 2022

Revised: 19 January 2023

Accepted: 30 January 2023

Published: 2 February 2023



Copyright: © 2023 by the authors. Licensee MDPI, Basel, Switzerland. This article is an open access article distributed under the terms and conditions of the Creative Commons Attribution (CC BY) license (<https://creativecommons.org/licenses/by/4.0/>).

1. Introduction

Mimicking biological procedures has always been a good approach to tackling energy questions. In recent years, numerous efforts have been made for the development of natural photosynthesis-inspired technologies for the efficient transformation of the energy from sunlight into chemical energy [1]. Hydrogen is considered an efficient energy vector due to the high energy density of the H₂ molecule (119 kJ/g) and its ability to be stored in large quantities. Furthermore, hydrogen combustion with air only produces water as residue, so it is considered a cyclic and environmentally friendly process [2].

Aiming at designing efficient hydrogen evolution catalysts, alternative to traditional Pt-based catalysts, the first studies were focused on simulating the activity of hydrogenase enzymes (especially metalloproteins) for hydrogen production [3,4]. In fact, hydrogenases utilizing earth-abundant metals such as Fe or Ni-Fe are the most active molecular catalysts for hydrogen production [5,6]. Although numerous studies have been performed on the design of biomimetic models of [Fe]-hydrogenases for hydrogen production, their inherent instability during the catalytic process has limited their applicability. In this sense, to solve these drawbacks, recent approaches have been focused on the assembly of biomimetic diiron catalysts on heterogeneous supports, such as metal organic frameworks (MOFs) [7], silica-based mesoporous materials [8] or graphene-based materials [9] for light-induced hydrogen production. These heterogeneous matrices have provided improved stability for the anchored molecular catalyst, overcoming those issues related to its water solubility and photostability [10].

Conversely, in the past decades, cobalt compounds have provided an appealing alternative to hydrogenase mimic complexes as efficient and low-cost HER catalysts. Inspired by the structure of vitamin B12 and more specifically in the stable organometallic cobalt complex, 5-deoxyadenosyl-(5,6-dimethylbenzimidazolyl)-cobinamide, present in its core [11], cobaloxime catalysts have been widely studied for electro and photocatalytic hydrogen production. Their great interest as molecular catalysts is given by their high O₂ tolerance [12,13], which allows their use under aerobic conditions, their facile synthesis, and their tunable catalytic properties only modifying the substituents on the equatorial and/or axial ligands [14,15]. Furthermore, they show high proton-reduction activity at moderately low overpotential [16] and can work in aqueous solutions [17].

Since the first example reported by Ziessel and co-workers about a cobaloxime complex for photocatalytic hydrogen production [18], numerous advances have been achieved in the design of more efficient molecular cobaloxime catalysts. Among them, one of the most interesting approaches to improve their catalytic activity is based on the heterogenization of such complexes and derivatives on solid supports. This approach is highly attractive because it improves the stability of the molecular catalysts while allowing their recyclability. Until now, most of the synthetic strategies used for that purpose have been focused on the development of materials containing surface pyridine moieties, which can act as ligands to axially coordinate a cobaloxime core. It is well documented that the catalytic properties of cobalt-diimine complexes can be improved by the presence of N-donor groups in the axial position [19]. In the last decades, several studies have revealed an increase in the electrocatalytic HER efficiency with cobaloximes assembled on the surface of carbon-based materials [20] and semiconductors [21].

Recently, this methodology has been extended to other non-conductive porous supports, such as metal organic frameworks (MOFs) [22,23], covalent organic frameworks (COFs) [24], and most recently, on periodic mesoporous organosilicas (PMOs) [25] for light-driven photocatalytic hydrogen production. Nevertheless, the major drawbacks and limitations of these molecular assemblies are the degradation of the equatorial ligand [26] and the de-coordination of the axial ligand [14] under catalytic conditions.

These findings indicate the relevance of considering enzyme-inspired outer coordination spheres (OCS) features around the cobalt core during the artificial catalyst design, therefore mimicking the protein scaffold of natural hydrogenases [27]. In this sense, initial studies reported by Wakerley and Reisner analyzed the influence of over 20 different substituted-pyridine ligands axially coordinated to a cobaloxime core for H₂ production. They found that the presence of more electron-donating pyridine ligands gave rise to an enhancement of the catalytic activity [15]. More recently, Dutta et al. [28] demonstrated that the improvement in the catalytic efficiency and long-term stability of a synthetic cobaloxime complex on electrocatalytic H₂ production was influenced by the number of basic groups on the outer coordination sphere of the cobaloxime core. Recently, these researchers extended the OCS studies to axial-imidazole-linked cobaloxime, one of the most active homogeneous cobalt complexes [29]. As previous results obtained by axial-pyridine-linked cobaloxime, the presence of peripheral basic functionalities around the same cobaloxime core enhanced the electro- and photocatalytic hydrogen production. These results show the relevance of the appropriated primary axial coordination sphere substituents to the catalytic cobalt center. It is important to note that most of the research in this field relies on the study of the electro- and photocatalytic HER performance of homogenous cobaloxime catalysts, with scarce studies on heterogenous systems.

In this context, our recently developed cobaloxime-PMO hybrid provides an approach for the design of heterogeneous cobaloxime systems [25]. In previous work, an efficient cobaloxime HER catalyst was synthesized through the coordination of a cobalt complex, $Co(dmgh_2)(dmgh)Cl_2$, on an ethylene-bridged periodic mesoporous organosilica (PMO) containing pyridine moieties. Compared to its homogenous counterparts, this system provided increased stability of the cobalt complex into the mesopores, which was reflected

in its enhanced catalytic efficiency. Until now, it was a unique example of anchoring cobaloxime HER catalysts on the surface of a PMO.

Herein, we report the synthesis of a novel cobaloxime-PMO hybrid material by axial coordination of a cobaloxime catalyst $[Co(dmgh_2)(dmgh)Cl_2]$ on the imidazole ligands present on the surface of an ethylene-bridged PMO. The hybrid system was fully characterized by different techniques and evaluated as a catalyst in the photocatalytic hydrogen evolution reaction.

2. Materials and Methods

2.1. Chemicals

The reagents for the synthesis of the different PMO materials, including octadecyltrimethylammonium bromide (OTAB, Sigma-Aldrich, Lyon, France), sodium hydroxide (NaOH, Sigma-Aldrich, Schnellendorf), 3-(chloropropyl)-triethoxysilane (95%, Sigma-Aldrich, Lyon, France), 1,2-bis(triethoxysilyl)ethane (96%, BTEE, Sigma-Aldrich, Lyon, France), and imidazole (99%, Sigma-Aldrich, Lyon, France), were used as received without further purification. Dimethylglyoxime (99%, Sigma-Aldrich, Lyon, France), acetone (>99.5%, Sigma-Aldrich, Lyon, France), cobalt (II) chloride hexahydrate (Acros Organics, Geel, Belgium), methanol (>99.9%, PanReac, Barcelona, Spain), imidazole (>99.9%, Sigma-Aldrich, Lyon, France), and chloroform (99.9%, Sigma-Aldrich, Lyon, France), employed for the synthesis of the cobalt complex, were used as supplied. Photocatalytic experiments were performed using acetonitrile (99.7%, PanReac, Barcelona, Spain) and Milli-Q-water as solvents, eosin Y (>95%, TCI, Zwijndrecht, Belgium) as photosensitizer and triethanolamine (>99%, TEOA, Sigma-Aldrich, Lyon, France) as a sacrificial electron donor.

2.2. Synthesis of the Materials

2.2.1. Synthesis of Cobaloxime Complexes: $Co(dmgh_2)(dmgh)Cl_2$ and $Co(dmgh)_2(Im)Cl$

$Co(dmgh_2)(dmgh)Cl_2$ complex was synthesized according to a previously reported procedure [30]. $CoCl_2 \cdot 6H_2O$ (2.1 mmol, 0.5 g) and dimethylglyoxime (4.2 mmol, 0.49 g) were dissolved in dry acetone (15 mL). The resulting solution was kept under stirring at room temperature for 30 min, after which it was filtered to eliminate any unreacted reactant. The filtrate was cooled overnight to form green crystals. These crystals were recovered by filtration and washed with cold acetone. The $Co(dmgh_2)(dmgh)Cl_2$ complex was dried under vacuum at 80 °C.

For the synthesis of the cobaloxime complex containing an axial imidazole ligand, $Co(dmgh_2)(dmgh)Cl_2$ complex (0.92 mmol, 0.33 g) was dispersed in 4 mL of chloroform and then the solution was stirred at room temperature for 10 min. Afterward, the imidazole ligand (2.28 mmol), previously dissolved in 4.5 mL of $CHCl_3$, was added dropwise to the solution. During this process, the green solution turned brown, indicating the ligand exchange had gone to completion. Subsequently, 3 mL of distilled H_2O was added to the solution, and it was stirred for 2 h. The aqueous phase was separated by decantation and the organic phase was washed with H_2O (3×15 mL). Finally, the product was washed with ethanol and dried under vacuum at 80 °C overnight. The final complex was named $Co(dmgh)_2(Im)Cl$ [19].

2.2.2. Synthesis of Chloropropyl Functionalized Ethylene-Bridged Periodic Mesoporous Organosilicas (Cl-EtPMO)

In a typical synthesis [31], the OTAB surfactant (0.85 g) was dissolved in a basic solution of NaOH (0.89 mL, 6 M) and Milli-Q water (53 mL). The solution was stirred overnight at 45 °C. Then, a mixture of organosilane precursors (2.04 mmol in total) in a molar ratio of 80% 1,2-bis(triethoxysilyl)ethane and 20% (3-chloropropyl)triethoxysilane was added dropwise under stirring. The resulting solution was stirred at the same temperature for 24 h. Afterward, the mixture was aged at 97 °C for 4 days under static conditions. The obtained solid was collected by filtration and thoroughly washed with water. In order to remove the surfactant, 1 g of as-synthesized material was refluxed in an ethanolic solution (50 mL of

ethanol with 1 mL of HCl 37 wt%) for 12 h. This procedure was repeated twice. The final material was filtered out and dried at 100 °C under vacuum. It was named Cl-EtPMO.

2.2.3. Anchoring of Imidazole on Cl-EtPMO

The functionalization of Cl-EtPMO material by imidazole groups was carried out following the procedure reported by Zhang et al. [32]. The material Cl-EtPMO (1.97 g) was dispersed in a solution of imidazole (0.18 g) in toluene (40 mL). The reaction mixture was stirred at 120 °C for 24 h, after which the solid was recovered by filtration and washed with toluene in order to remove the excess imidazole not anchored in the PMO structure. The final material was dried at 80 °C under vacuum overnight. The functionalized material was named Im-EtPMO.

2.2.4. Immobilization of Dichlorocobaloxime on Im-EtPMO

The immobilization of dichlorocobaloxime complex on the PMO structure through imidazole groups was carried out with the following procedure: Im-EtPMO (0.5 g) was dispersed in methanol (10 mL) and then, dichlorocobaloxime complex (0.3 g) was added to the solution. The resulting mixture was stirred at 80 °C for 24 h. Afterward, the solution was filtered and washed with methanol in order to remove the excess dichlorocobaloxime complex. The final product was dried at 80 °C under vacuum. The heterogenous catalyst was named Im-EtPMO-Co.

2.3. Physicochemical Characterization

X-ray powder diffraction (XRD) patterns were collected on a Bruker D8 Discover A25 diffractometer using Cu K α radiation. High-resolution transmission electron microscopy images were recorded on a JEOL JEM 1400 microscope. N₂ adsorption–desorption isotherms were recorded at –196 °C using an Autosorb-iQ MP/MP-XR instrument. Before measurement, all the samples were outgassed overnight at 100 °C. The surface area was calculated using the Brunauer–Emmett–Teller (BET) method and the pore size distribution was determined using the Density Functional Theory (DFT) method. The solid-state ¹³C CP/MAS NMR spectra were recorded on a Bruker Avance III HD 400 WB spectrometer at 13 kHz. The excitation pulse and recycle time for ¹³C CP/MAS NMR were 3.6 ms and 2 s, respectively. Chemical shifts were referenced to the tetramethylsilane (TMS) standard. Raman spectra of the samples were collected with a Renishaw Raman instrument with green laser light (532 nm). X-ray photoelectron spectroscopy (XPS) was performed on a SPECS Phoibos HAS 3500 150 MCD X-ray photoelectron spectrometer with a monochromatic Al anode (1486.7 eV). Regions were calibrated using the reference value BE (C1s) = 284.8 eV. Inductively coupled plasma mass spectrometry (ICP-MS) for the ⁵⁹Co isotope was measured using a NexION 350X spectrometer. Before the measurement, the sample was digested in an UltraWave microwave system.

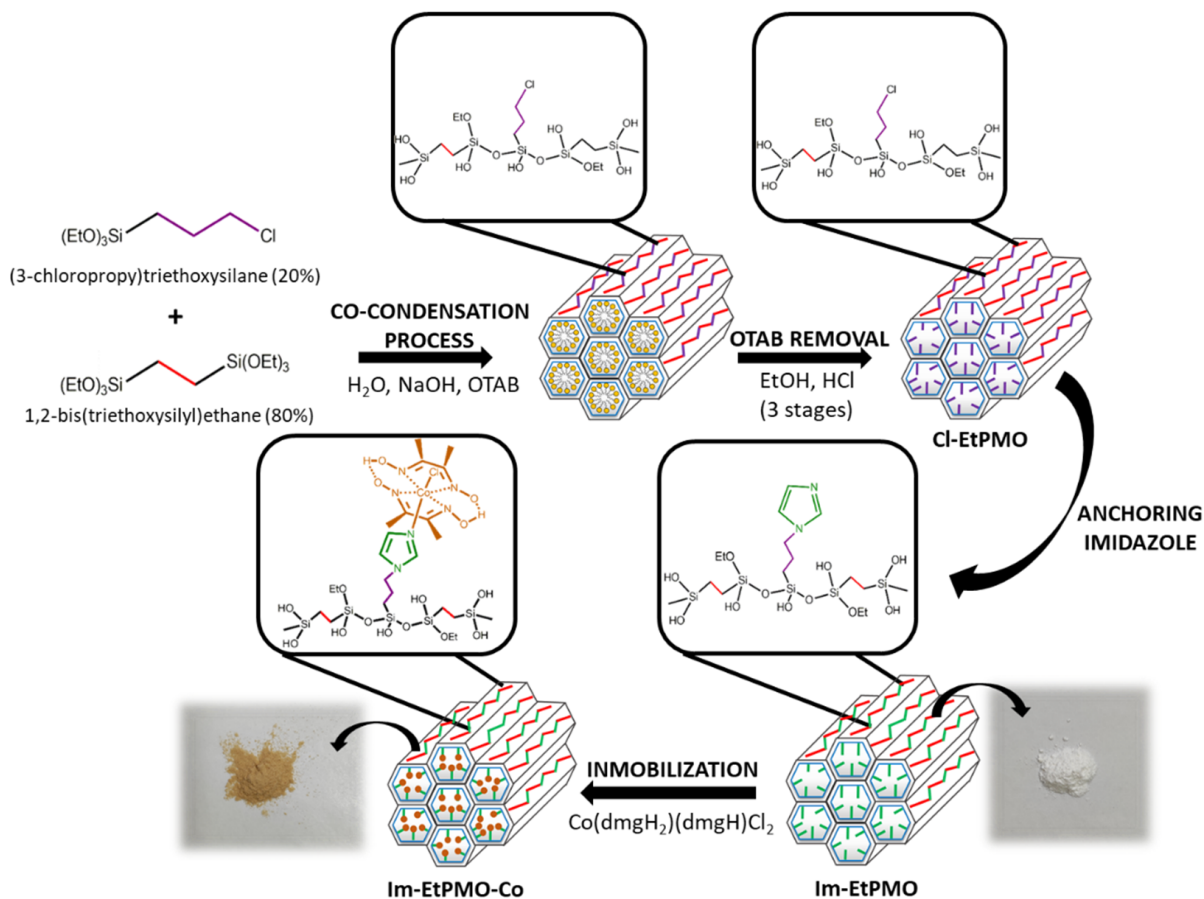
2.4. Photocatalytic Hydrogen Production Tests

Light-driven photocatalytic hydrogen production was carried out in a Restek vial (20 mL) with constant stirring under visible-light irradiation using a 300W Xe lamp (ORIEL) equipped with a Newport filter (FSQGC400, $\lambda \geq 400$ nm), at 10 cm distance. In a typical reaction, 1 mg of Im-EtPMO-Co catalyst was suspended in 11.4 mL of CH₃CN:H₂O (1:1) solution containing TEOA (10%) and eosin Y (0.05 mM). The pH of the reaction was adjusted to 7.4 with HCl (37 wt%). Subsequently, the solution was degassed bubbling N₂ for 30 min and irradiated with a Xe lamp. Sample aliquots (50 μ L) were taken at different reaction times using a gas-tight syringe and quantified by using a gas chromatograph (Shimadzu GC-2010 Plus) equipped with a barrier discharge ionization detector (BID) and a ShinCarbon ST column (2 m \times 2 mm i.d.). For the homogeneous catalyst, 1 mg of the molecular catalyst, *Co(dmgh)₂(Im)Cl*, was dispersed in 1:1 CH₃CN/H₂O (11.4 mL) containing EY (0.05 mM) and TEOA (10%), and the pH was adjusted with HCl to 7.4.

3. Results and Discussion

3.1. Synthetic Strategy for Cobaloxime-Tethered Imidazole-Functionalized Ethylene-Bridged PMO Catalyst

The approach proposed for the development of a novel cobaloxime-PMO hybrid catalyst is shown in Scheme 1. As can be observed, several steps were strictly needed to achieve the functionality required on the pore channels of the PMO material due to the non-availability of a functional mono-silane precursor with imidazole groups. For that, self-assembly assisted co-condensation reaction of a conventional bis-silane precursor, 1,2-bis(triethoxysilyl)ethane (BTEE), and chloropropyltriethoxysilane in the presence of OTAB as surfactant under basic conditions led to an ordered ethylene-bridged PMO with chloropropyl groups attached to the pore walls. Subsequently, the nucleophilic substitution of chlorine atoms by imidazole accompanied by the release of HCl gave rise to a PMO support containing imidazole groups on their pore channels. These organic groups can act as attachment points to further assemble cobaloxime catalysts on the surface of the PMO. To corroborate it, pictures depicted in Scheme 1 of the support before and after the immobilization of the cobaloxime complex clearly reflected the color change of the solid from white to light-brown produced by the anchoring of the molecular cobaloxime catalyst on the imidazole groups present on the PMO channels.



Scheme 1. Synthetic strategy of Im-EtPMO-Co catalyst.

3.2. Structural Characterization

The powder X-Ray diffraction (PXRD) patterns of all synthesized materials are depicted in Figure 1. The parent material (Cl-EtPMO) showed three reflection peaks in the low-angle region ($2\theta < 5^\circ$). The first diffraction peak at 1.78° corresponded to the (100) reflection with a d-spacing of 5 nm. The two second-order peaks were attributed to the (110) and (200) reflections with d-spacing of 2.9 and 2.5 nm, respectively. These diffraction

peaks are characteristics of 2D-hexagonal ordered ($p6mm$) mesostructures [33]. After functionalization by imidazole, the resulting Im-EtPMO material exhibited a similar diffraction pattern. Likewise, the subsequent anchoring of cobaloxime molecular catalyst through imidazole ligands preserved the initial ordered mesostructure.

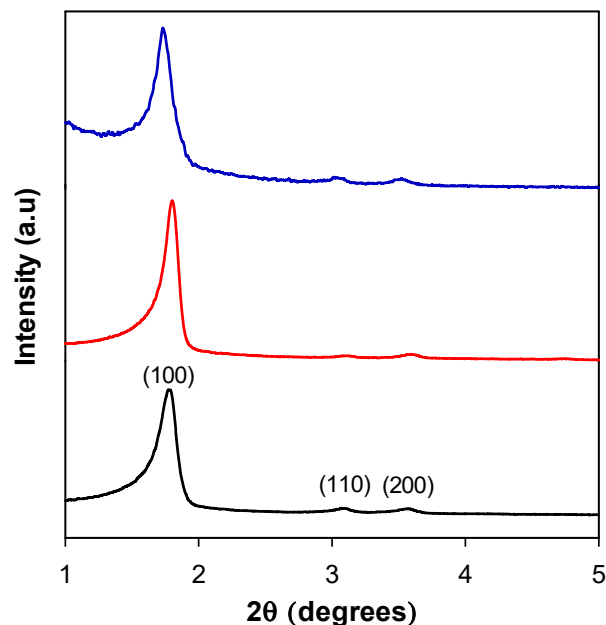


Figure 1. PXRD of Cl-EtPMO (black line), Im-EtPMO (red line), and Im-EtPMO-Co (blue line).

Transmission electron microscopy (TEM) images of Cl-EtPMO, Im-EtPMO, and Im-EtPMO-Co materials are depicted in Figure 2. TEM images showed that all PMO materials had highly ordered structures with uniform and parallel channel pores, which confirmed the findings obtained by XRD.

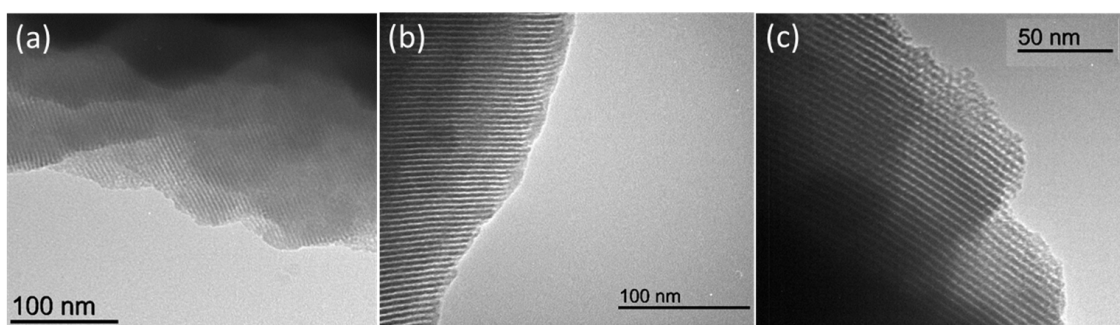


Figure 2. TEM images of Cl-EtPMO (a), Im-EtPMO (b), and Im-EtPMO-Co (c).

Im-EtPMO and Im-EtPMO-Co materials exhibited type-IV isotherms according to the IUPAC [34] with a condensation step at $P/P_0 = 0.3-0.7$, characteristic of mesoporous materials (Figure 3). Both materials showed a non-distinctive hysteresis loop, which is typical of materials with small mesopores [35]. The narrow pore size distribution and average pore size confirmed pores in the meso range. Table 1 summarizes the textural properties of the materials. Im-EtPMO showed a BET surface area, pore volume, and pore diameter of $583 \text{ m}^2 \text{ g}^{-1}$, $0.5 \text{ cm}^3 \text{ g}^{-1}$, and 4.2 nm , respectively. The anchoring of the molecular cobaloxime catalyst on the pendant imidazole groups gave rise to a slight decrease in surface area and pore volume.

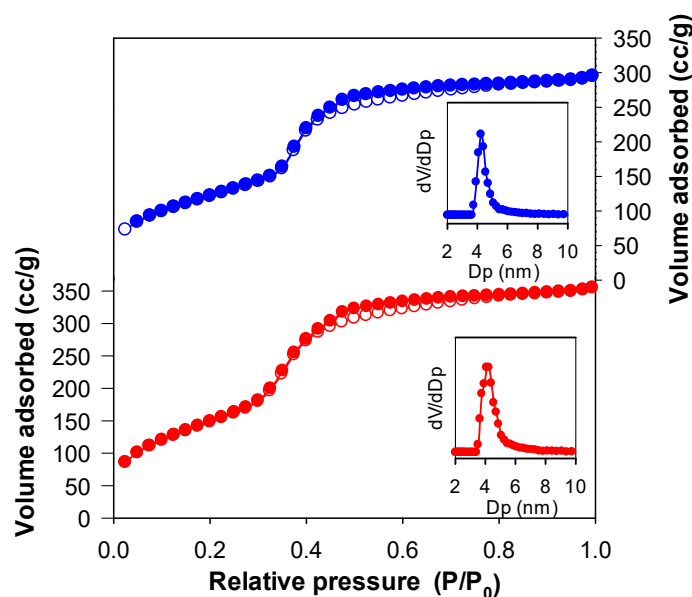


Figure 3. Nitrogen adsorption–desorption isotherms and pore size distributions (inset) of Im-EtPMO (red line) and Im-EtPMO-Co (blue line).

Table 1. Physicochemical properties of Im-EtPMO and Im-EtPMO-Co materials.

Sample	a_0^a (nm)	S_{BET} ($\text{m}^2 \text{g}^{-1}$)	V_p ($\text{cm}^3 \text{g}^{-1}$)	D_p^b (nm)	w^c (nm)
Im-EtPMO	5.6	583	0.52	4.2	5.6
Im-EtPMO-Co	5.7	455	0.43	4.2	5.7

^a Unit cell parameter calculated as $a_0 = 2d_{100}/\sqrt{3}$. ^b Calculated from DFT analysis. ^c Determined from the difference between $a_0 - D_p$.

The ^{13}C CP/MAS NMR measurements confirmed the presence of the organic bridging groups in the silica framework as well as the different organic groups anchored on the mesochannels (Figure 4). The Cl-EtPMO material showed an intense peak centered at 6 ppm associated with the Csp^3 of the ethylene groups present in the pore walls [36]. Small peaks at 50, 26, and 9 ppm correspond to the three carbon atoms in the chloroalkyl chain. The additional peaks at 58 and 17 ppm, corresponding to the $-\text{OCH}_2-$ and $-\text{CH}_3$ groups, respectively, derived from the incomplete hydrolysis of the ethoxy groups under synthesis conditions. After functionalization with imidazole, Im-EtPMO material showed new signals at low fields (136 and 123 ppm) attributed to the Csp^2 in the imidazole ring [37]. After immobilization of the cobaloxime complex on the surface of the PMO-containing imidazole groups, signals associated with $\text{C}=\text{N}$ (154 ppm) and $-\text{CH}_3$ (13 ppm) groups from the glyoximate ligands were clearly present [38]. Additionally, an aromatic signal at 130 ppm confirmed the coordination of nitrogen to cobalt atoms. The signal at 50 ppm is assigned to residual CH_3OH employed in the washing process to remove unreacted cobaloxime complex. These results were further confirmed by Raman spectroscopy.

Raman spectra of all synthesized materials are shown in Figure 5. Cl-EtPMO showed intense signals below 3000 cm^{-1} , associated with the C-H stretching of propyl chains as well as the ethylene bridges. After substitution with imidazole, the resulting material exhibited new signals above 3000 cm^{-1} attributed to $=\text{C}-\text{H}$ stretching vibration from the imidazole ring. Additionally, peaks in the region of $1500\text{--}1400 \text{ cm}^{-1}$ were associated with the $\text{C}=\text{C}$ and $\text{C}=\text{N}$ stretching vibrations of imidazole moieties [39,40]. After the immobilization of the cobaloxime complex, new vibrations at 1620 and 1220 cm^{-1} were assigned to $\text{C}=\text{N}$ and $\text{N}-\text{O}$ stretching vibrations, respectively, for dimethylglyoxime groups of the cobaloxime [41].

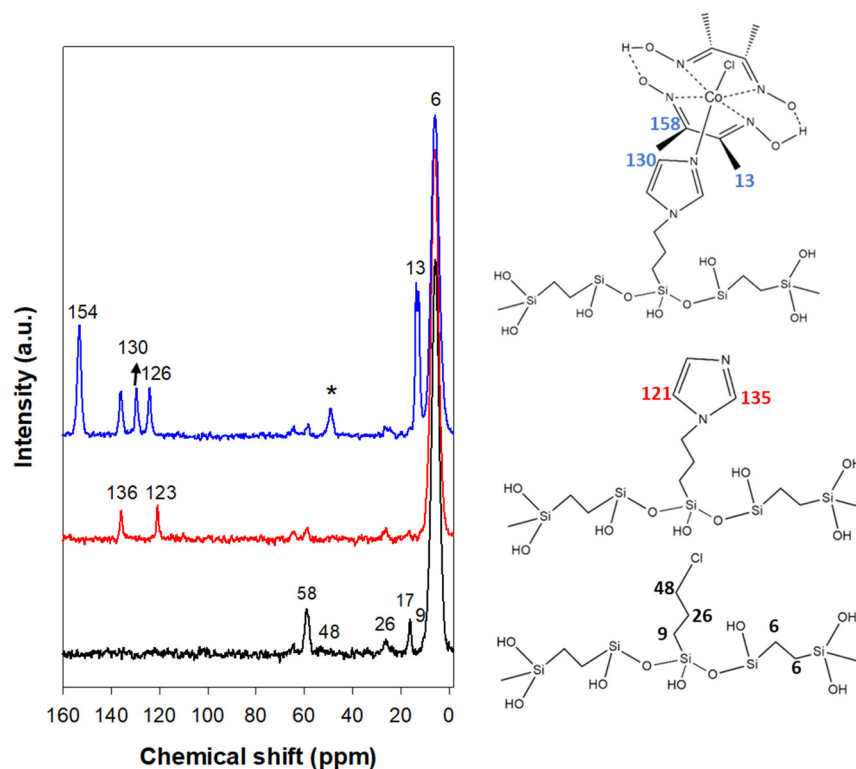


Figure 4. ^{13}C CP/MAS NMR spectra of Cl-EtPMO (black line), Im-EtPMO (red line), and Im-EtPMO-Co (blue line). Predicted chemical shifts on the right. *—low field.

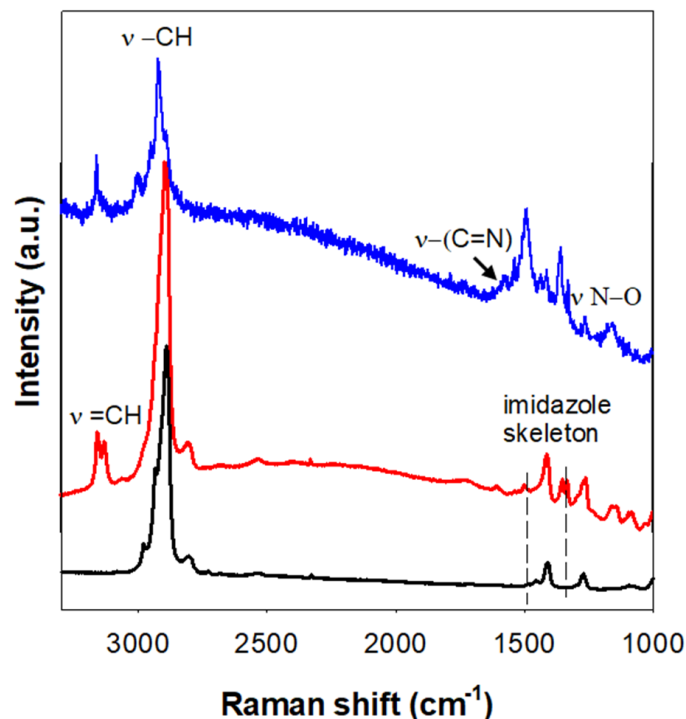


Figure 5. Raman spectra of Cl-EtPMO (black line), Im-EtPMO (red line), and Im-EtPMO-Co (blue line).

X-ray photoelectron spectroscopy (XPS) measurements provided evidence about the incorporation of cobaloxime catalyst on the surface of PMO as well as the oxidation state of the cobalt species (Figure 6). The survey spectrum of Im-EtPMO showed peaks related to O, C, N, Cl, and Si elements. After the immobilization of the cobaloxime catalyst, an

additional peak associated with the Co element was present. The N1s high-resolution spectrum of Im-EtPMO showed a broad peak around 400.8 eV, which was attributed to the nitrogen atoms present on the imidazole ring (Figure 6a) [42,43]. A similar N1s XPS spectrum was obtained for Im-EtPMO-Co, but with the maximum slightly shifted towards lower binding energy (400.3 eV). This peak would encompass the pyridinic-N coordinated to the Co centers, the N-C groups present on the imidazole groups, as well as the N=C bonds from the glyoximate ligands of the cobaloxime. Furthermore, the study of the Co 2p region (810–770 eV) clearly evidenced the presence of cobalt species in the Im-EtPMO-Co sample (Figure 6b). The high-resolution Co2p spectrum exhibited two symmetrical doublet peaks at 781 and 796 eV corresponding to the $2p_{3/2}$ and $2p_{1/2}$ levels in a 2:1 expected ratio [44]. The 15.0 eV of distance and the lack of satellite bands undoubtedly evidenced the presence of cobalt in a +3 oxidation state in the cobaloxime complex [45].

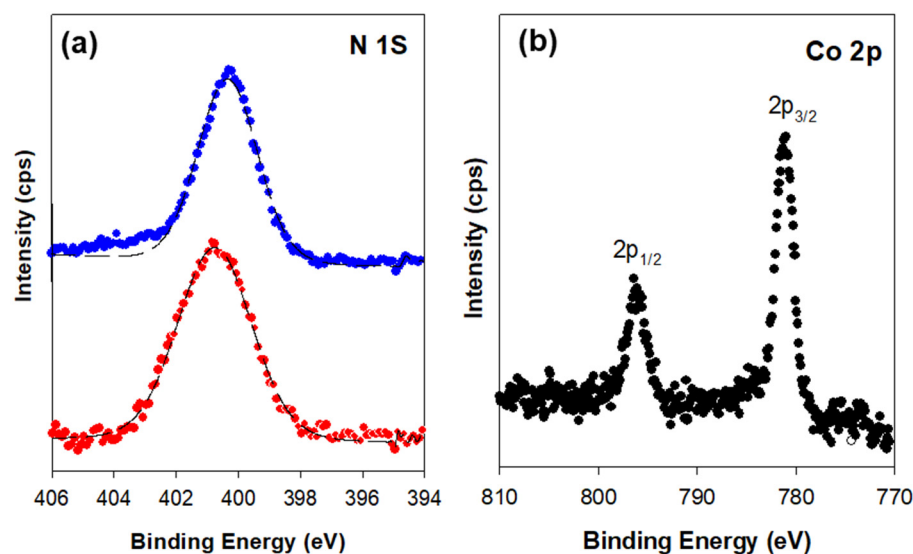
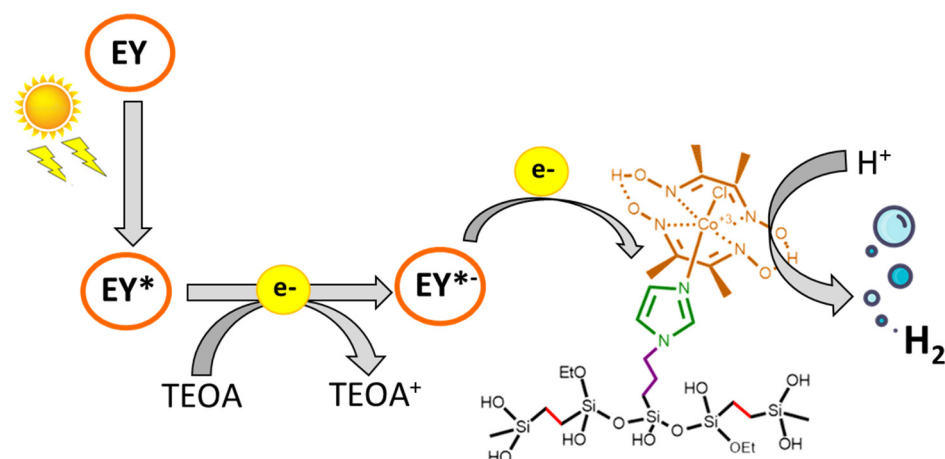


Figure 6. (a) High-resolution XPS spectra of N1s for Im-EtPMO (red line) and Im-EtPMO-Co (blue line). (b) High-resolution Co2p XPS spectrum for Im-EtPMO-Co.

The functionalization degree of Cl-EtPMO material by imidazole was analyzed by elemental analysis. The nitrogen content for Im-EtPMO was 1.38 mmol g^{-1} . After the immobilization of the cobalt complex via the cobalt-imidazole axial bond, the cobalt loading analyzed by ICP-MS was 0.70 mmol g^{-1} . According to these results, the N/Co ratio on the Im-EtPMO-Co catalyst was ca. 2.0. It means that one cobaloxime complex was coordinated per imidazole group on the PMO support. These findings revealed that all surface imidazole ligands were completely accessible and acted as attachment points to assemble the cobaloxime catalyst.

3.3. Photocatalytic Hydrogen Evolution Reaction

Once the successful anchoring of the cobaloxime catalyst via axial ligation of imidazole groups present on the surface of the PMO support was confirmed, 1 mg of Im-EtPMO-Co catalyst was assessed towards H_2 production in a water: acetonitrile solution under continuous visible light irradiation ($>400 \text{ nm}$) in the presence of eosin Y and TEOA as photosensitizer and electron donor, respectively. According to the literature, as depicted in Scheme 2, the photocatalytic hydrogen evolution reaction commences with the reductive quenching of photoexcited [EY]. Subsequently, $[\text{EY}^{*-}]$ reductant transfers an electron to the proton reduction catalyst (Im-EtPMO-Co) to produce hydrogen.



Scheme 2. Schematic representation of photocatalytic hydrogen evolution reaction with TEOA and Eosin Y (EY) as electron donor and photosensitizer, respectively. (EY*, photoexcited EY).

Previous similar works had shown that all components—photosensitizer, electron donor, and catalyst—were strictly necessary to carry out the hydrogen evolution reaction [25]. Figure 7a depicts the catalytic HER turnover numbers (TON) (vs [Co]) after 4 h of irradiation. As can be observed, our catalytic system demonstrated photocatalytic H₂ production with an initial rate of 68.1 mmol h⁻¹ g⁻¹. The HER was leveled off after 2.5 h of irradiation, reaching a hydrogen production maximum of 95 mmol g⁻¹. This corresponded to a TON (vs [Co]) of 138. The photocatalytic activity was optimized by increasing the amount of catalyst from 1 mg to 3.6 mg. Under similar reaction conditions, a gradual drop in hydrogen production was observed by increasing the concentration of Im-EtPMO-Co in the system. The TON decreased from 138 (1 mg catalyst) to 109 (1.5 mg), 94 (2 mg), and 54 (3.6 mg). In light-induced hydrogen production systems, an increase in the amount of solid catalyst is accompanied by a decrease in the amount of H₂ generated due to the blocking of light radiation by the catalyst particles [8,46,47].

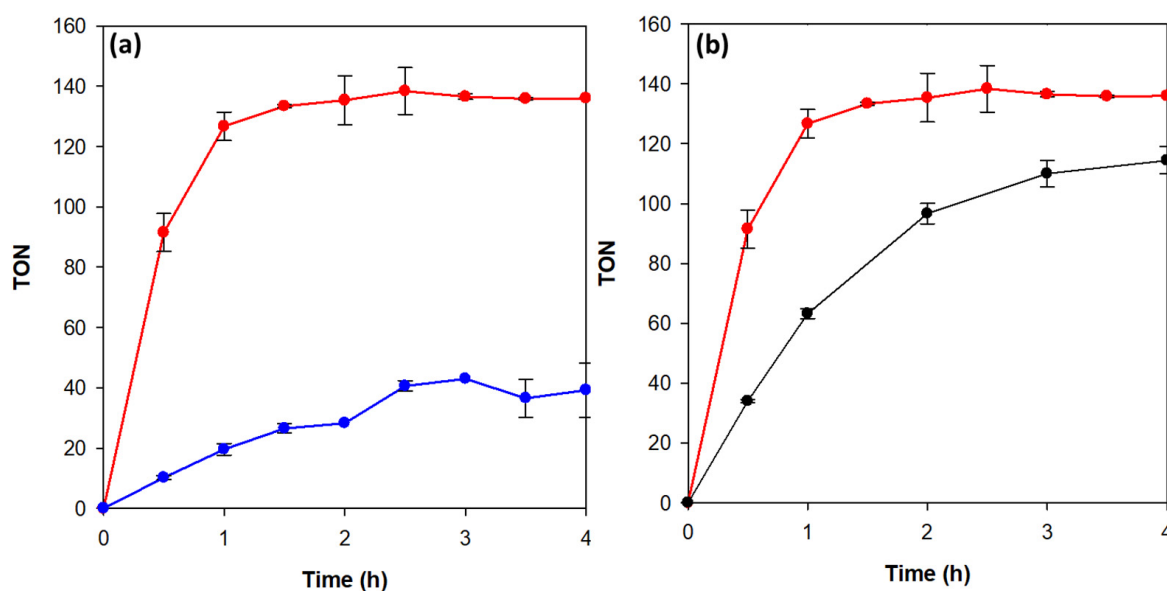


Figure 7. (a) Photocatalytic HER with Im-EtPMO-Co (red line) and Co(dmgh)₂(Im)Cl homogeneous catalyst (blue line). (b) Photocatalytic HER with Im-EtPMO-Co (red line) and py-etPMO-Co (black line) as catalysts.

For comparison, Co(dmgh)₂(Im)Cl complex was tested as a homogenous catalyst under analogous reaction conditions. After 2.5 h, the total amount of evolved hydrogen

corresponded to a TON (vs [Co]) of 40. This value was in the range of that reported by Dolui et al. [29] for the same homogenous chloro-imidazole cobaloxime complex. These results clearly reflected an increase in the photocatalytic activity of the molecular cobaloxime catalyst after its immobilization on a PMO material. Previous reports have attributed the activity enhancement undergone by immobilized cobaloxime catalysts, compared to their homogenous counterparts, to the confinement of the molecular catalysts into pores of the material [23,24]. It is well known that cobaloximes are degraded under photocatalytic conditions due to the decoordination of the N-donating ligand from the cobaloxime core. Although this fact would limit the stability of the cobaloxime species in a solution capable of being reduced, the possible re-coordination of these species to the N-donating ligands present in the pores of the material would lead to the reactivation of the cobaloxime center.

Finally, aiming at proving the role of the primary axial coordination sphere in cobaloxime complexes on HER, our proposed system, Im-EtPMO-Co, was compared with a recently reported cobaloxime-hybrid PMO, py-etPMO-Co. In this system, the cobaloxime units were assembled via a cobalt-pyridine axial bond on the porous channels of the PMO [25]. Under the same photochemical conditions, the py-etPMO-Co catalyst was less active for the photoinduced hydrogen evolution, reaching a TON (vs [Co]) of 80 (Figure 7b). This lower hydrogen production can be explained on the basis of the basicity of N-aromatic ligands coordinated with the cobaloxime catalyst. It is reported that a higher pKa of axial N-based aromatic ligands is directly correlated with a higher stability and activity of the corresponding catalyst [14]. On this basis, the higher pKa of N-alkyl imidazole ligand compared to the pyridine one resulted in a higher photocatalytic HER activity of N-methyl imidazole-linked cobaloximes in comparison to axial pyridine-linked cobaloximes.

4. Conclusions

In this work, we present a novel cobaloxime-PMO hybrid synthesized by axial coordination of the cobaloxime core onto the imidazole groups present on the surface of an ethylene-bridged periodic mesoporous organosilica. The cobaloxime hydrogen evolution catalyst was evaluated in the photocatalytic hydrogen production in presence of eosin Y and TEOA, as photosensitizer and electron donor, respectively. This catalytic system reached a hydrogen production maximum of 95 mmol g^{-1} , which corresponded to a TON (vs [Co]) of 138. This value largely exceeded that obtained by its homogenous counterpart, therefore corroborating the positive confinement effect of the molecular cobaloxime catalyst in the pores of the PMO material. Likewise, the existence of an axial cobalt-imidazole ligation on this system led to an enhanced photocatalytic hydrogen production compared to a previously reported cobaloxime-PMO hybrid with cobalt-pyridine ligation.

Author Contributions: Conceptualization, M.Á.N., F.J.R.-S. and D.E.; investigation, M.Á.N. and M.A.M.; writing—original draft preparation, M.Á.N.; writing—review and editing, M.Á.N., M.A.M., C.J.-S., J.R.R., F.J.R.-S. and D.E.; supervision, F.J.R.-S. and D.E. All authors have read and agreed to the published version of the manuscript.

Funding: This research was funded by Fundación Ramón Areces (RAMON ARECES 16), Ministerio de Ciencia e Innovación (projects RTI2018-101611-B-I00 and PDC2022-133973-I00), and Consejería de Universidad, Investigación e Innovación from Junta de Andalucía (Project ProyExcel_00492).

Data Availability Statement: Not applicable.

Acknowledgments: The authors are grateful to the Fundación Ramón Areces, Ministerio de Ciencia e Innovación (Projects RTI2018-101611-B-I00 and PDC2022-133973-I00), Consejería de Universidad, Investigación e Innovación from Junta de Andalucía (Project ProyExcel_00492 and FQM-346) and Feder Funds for financial support. The technical support from IQUEMA and SCAI is greatly appreciated.

Conflicts of Interest: The authors declare no conflict of interest.

References

1. Nocera, D.G. The Artificial Leaf. *Acc. Chem. Res.* **2012**, *45*, 767–776. [[CrossRef](#)] [[PubMed](#)]
2. Koroneos, C.; Dompros, A.; Roumbas, G.; Moussiopoulos, N. Life Cycle Assessment of Hydrogen Fuel Production Processes. *Int. J. Hydrog. Energy* **2004**, *29*, 1443–1450. [[CrossRef](#)]
3. Le Goff, A.; Artero, V.; Jusselme, B.; Tran, P.D.; Guillet, N.; Métayé, R.; Fihri, A.; Palacin, S.; Fontecave, M. From Hydrogenases to Noble Metal-Free Catalytic Nanomaterials for H₂ Production and Uptake. *Science* **2009**, *326*, 1384–1387. [[CrossRef](#)]
4. Gao, S.; Fan, W.; Liu, Y.; Jiang, D.; Duan, Q. Artificial Water-Soluble Systems Inspired by [FeFe]-Hydrogenases for Electro- and Photocatalytic Hydrogen Production. *Int. J. Hydrog. Energy* **2020**, *19*, 4305–4327. [[CrossRef](#)]
5. Lu, Y.; Koo, J. O₂ Sensitivity and H₂ Production Activity of Hydrogenases—A Review. *Biotechnol. Bioeng.* **2019**, *116*, 3124–3135. [[CrossRef](#)]
6. Azwar, M.Y.; Hussain, M.A.; Abdul-wahab, A.K. Development of Biohydrogen Production by Photobiological, Fermentation and Electrochemical Processes: A Review. *Renew. Sustain. Energy Rev.* **2014**, *31*, 158–173. [[CrossRef](#)]
7. Pullen, S.; Fei, H.; Orthaber, A.; Cohen, S.M.; Ott, S. Enhanced Photochemical Hydrogen Production by a Molecular Diiron Catalyst Incorporated into a Metal-Organic Framework. *J. Am. Chem. Soc.* **2013**, *135*, 16997–17003. [[CrossRef](#)]
8. Himiyama, T.; Waki, M.; Esquivel, D.; Onoda, A.; Hayashi, T.; Van Der Voort, P.; Inagaki, S. A Heterogeneous Hydrogen-Evolution Catalyst Based on a Mesoporous Organosilica with a Diiron Catalytic Center Modelling [FeFe]-Hydrogenase. *ChemCatChem* **2018**, *10*, 4908–4913. [[CrossRef](#)]
9. Li, R.-X.; Ren, X.-T.; Tang, M.-Y.; Chen, M.-X.; Huang, G.-B.; Fang, C.-H.; Liu, T.; Feng, Z.-H.; Yin, Y.-B.; Guo, Y.-M.; et al. Fabrication of Covalently Linked Graphene-Mediated [FeFe]-Hydrogenases Biomimetic Photocatalytic Hydrogen Evolution System in Aqueous Solution. *Appl. Catal. B Environ.* **2018**, *224*, 772–782. [[CrossRef](#)]
10. Amaro-Gahete, J.; Pavliuk, M.V.; Tian, H.; Esquivel, D.; Romero-Salguero, F.J.; Ott, S. Catalytic Systems Mimicking the [FeFe]-Hydrogenase Active Site for Visible-Light-Driven Hydrogen Production. *Coord. Chem. Rev.* **2021**, *448*, 214172. [[CrossRef](#)]
11. Gerhard, N. Schrauzer Organocobalt Chemistry of Vitamin B₁₂ Model Compounds (Cobaloximes). *Acc. Chem. Res.* **1968**, *1*, 97–103.
12. Lakadamyali, F.; Kato, M.; Muresan, N.M.; Reisner, E. Selective Reduction of Aqueous Protons to Hydrogen with a Synthetic Cobaloxime Catalyst in the Presence of Atmospheric Oxygen. *Angew. Chem.-Int. Ed.* **2012**, *51*, 9381–9384. [[CrossRef](#)]
13. Wakerley, D.W.; Gross, M.A.; Reisner, E. Proton Reduction by Molecular Catalysts in Water under Demanding Atmospheres. *Chem. Commun.* **2014**, *50*, 15995–15998. [[CrossRef](#)] [[PubMed](#)]
14. Willkomm, J.; Muresan, N.M.; Reisner, E. Enhancing H₂ Evolution Performance of an Immobilised Cobalt Catalyst by Rational Ligand Design. *Chem. Sci.* **2015**, *6*, 2727–2736. [[CrossRef](#)] [[PubMed](#)]
15. Wakerley, D.W.; Reisner, E. Development and Understanding of Cobaloxime Activity through Electrochemical Molecular Catalyst Screening. *Phys. Chem. Chem. Phys.* **2014**, *16*, 5739–5746. [[CrossRef](#)] [[PubMed](#)]
16. Artero, V.; Pe, J.; Fontecave, M. Cobalt and Nickel Diimine-Dioxime Complexes as Molecular Electrocatalysts for Hydrogen Evolution with Low Overvoltages. *Proc. Natl. Acad. Sci. USA* **2009**, *106*, 20627–20632.
17. Andreiadis, E.S.; Jacques, P.A.; Tran, P.D.; Leyris, A.; Chavarot-Kerlidou, M.; Jusselme, B.; Matheron, M.; Pécaut, J.; Palacin, S.; Fontecave, M.; et al. Molecular Engineering of a Cobalt-Based Electrocatalytic Nanomaterial for H₂ Evolution under Fully Aqueous Conditions. *Nat. Chem.* **2013**, *5*, 48–53. [[CrossRef](#)] [[PubMed](#)]
18. Hawecker, J.; Lehn, J.M.; Zissel, R. Efficient Homogeneous Photochemical Hydrogen Generation and Water Reduction Mediated by Cobaloxime or Macrocyclic Cobalt Complexes. *Nouv. J. Chim.* **1983**, *7*, 271–277. [[CrossRef](#)]
19. Panagiotopoulos, A.; Ladomenou, K.; Sun, D.; Artero, V.; Coutsolelos, A.G. Photochemical Hydrogen Production and Cobaloximes: The Influence of the Cobalt Axial N-Ligand on the System Stability. *Dalt. Trans.* **2016**, *45*, 6732–6738. [[CrossRef](#)]
20. Sideri, I.K.; Charalambidis, G.; Coutsolelos, A.G.; Arenal, R.; Tagmatarchis, N. Pyridine vs. Imidazole Axial Ligation on Cobaloxime Grafted Graphene: Hydrogen Evolution Reaction Insights. *Nanomaterials* **2022**, *12*, 3077. [[CrossRef](#)]
21. Wadsworth, B.L.; Nishiori, D.; Nguyen, N.P.; Cruz, E.A.R. Electrochemistry of Polymeric Cobaloxime-Containing Assemblies in Organic and Aqueous Solvents. *ECSS J. Solid State Sci. Technol.* **2020**, *9*, 061018. [[CrossRef](#)]
22. Roy, S.; Huang, Z.; Bhunia, A.; Castner, A.; Gupta, A.K.; Zou, X.; Ott, S. Electrocatalytic Hydrogen Evolution from a Cobaloxime-Based Metal-Organic Framework Thin Film. *J. Am. Chem. Soc.* **2019**, *141*, 15942–15950. [[CrossRef](#)] [[PubMed](#)]
23. Roy, S.; Bhunia, A.; Schuth, N.; Haumann, M.; Ott, S. Light-Driven Hydrogen Evolution Catalyzed by a Cobaloxime Catalyst Incorporated in a MIL-101(Cr) Metal-Organic Framework. *Sustain. Energy Fuels* **2018**, *2*, 1148–1152. [[CrossRef](#)] [[PubMed](#)]
24. Gottschling, K.; Savasci, G.; Vignolo-González, H.; Schmidt, S.; Mauker, P.; Banerjee, T.; Rovó, P.; Ochsenfeld, C.; Lotsch, B.V. Rational Design of Covalent Cobaloxime-Covalent Organic Framework Hybrids for Enhanced Photocatalytic Hydrogen Evolution. *J. Am. Chem. Soc.* **2020**, *142*, 12146–12156. [[CrossRef](#)]
25. Navarro, M.Á.; Cosano, D.; Bhunia, A.; Simonelli, L.; Martin-Diaconescu, V.; Romero-Salguero, F.J.; Esquivel, D. Cobaloxime Tethered Pyridine-Functionalized Ethylene-Bridged Periodic Mesoporous Organosilica as an Efficient HER Catalyst. *Sustain. Energy Fuels* **2022**, *6*, 398–407. [[CrossRef](#)]
26. McCormick, T.M.; Han, Z.; Weinberg, D.J.; Brennessel, W.W.; Holland, P.L.; Eisenberg, R. Impact of Ligand Exchange in Hydrogen Production from Cobaloxime-Containing Photocatalytic Systems. *Inorg. Chem.* **2011**, *50*, 10660–10666. [[CrossRef](#)]
27. Dolui, D.; Khandelwal, S.; Majumder, P.; Dutta, A. The Odyssey of Cobaloximes for Catalytic H₂ production and Their Recent Revival with Enzyme-Inspired Design. *Chem. Commun.* **2020**, *56*, 8166–8181. [[CrossRef](#)] [[PubMed](#)]

28. Dolui, D.; Khandelwal, S.; Shaik, A.; Gaat, D.; Thiruvengatam, V.; Dutta, A. Enzyme-Inspired Synthetic Proton Relays Generate Fast and Acid-Stable Cobalt-Based H₂ Production Electrocatalysts. *ACS Catal.* **2019**, *9*, 10115–10125. [[CrossRef](#)]
29. Dolui, D.; Das, S.; Bharti, J.; Kumar, S.; Kumar, P.; Dutta, A. Bio-Inspired Cobalt Catalyst Enables Natural-Sunlight-Driven Hydrogen Production from Aerobic Neutral Aqueous Solution. *Cell Rep. Phys. Sci.* **2020**, *1*, 100007. [[CrossRef](#)]
30. Trogler, W.C.; Stewart, R.C. Cis and Trans Effects on the Proton Magnetic Resonance Spectra of Cobaloximes. *Inorg. Chem.* **1974**, *13*, 1564–1570. [[CrossRef](#)]
31. Waki, M.; Mizoshita, N.; Tani, T.; Inagaki, S. Periodic Mesoporous Organosilica Derivatives Bearing a High Density of Metal Complexes on Pore Surfaces. *Angew. Chem.-Int. Ed.* **2011**, *50*, 11667–11671. [[CrossRef](#)]
32. Zhang, P.; Sun, Y.; Zhang, Q.; Guo, Y.; Song, D. Upgrading of Pyrolysis Biofuel via Esterification of Acetic Acid with Benzyl Alcohol Catalyzed by Brønsted Acidic Ionic Liquid Functionalized Ethyl-Bridged Organosilica Hollow Nanospheres. *Fuel* **2018**, *228*, 175–186. [[CrossRef](#)]
33. Xia, Y.; Mokaya, R. To Stir or Not to Stir: Formation of Hierarchical Superstructures of Molecularly Ordered Ethylene-Bridged Periodic Mesoporous Organosilicas. *J. Mater. Chem.* **2006**, *16*, 395–400. [[CrossRef](#)]
34. Sing, K.S.W. Reporting Physisorption Data for Gas / Solid Systems with Special Reference to the Determination of S. *Pure Appl. Chem.* **1982**, *54*, 2201–2218. [[CrossRef](#)]
35. Liu, W.; Kaczmarek, A.M.; Folens, K.; Du Laing, G.; Van Der Voort, P.; Van Deun, R. Rational Design of Lanthanide Nano Periodic Mesoporous Organosilicas (Ln-Nano-PMOs) for near-Infrared Emission. *Dalt. Trans.* **2021**, *50*, 2774–2781. [[CrossRef](#)]
36. Navarro, M.Á.; Amaro-Gahete, J.; Ruiz, J.R.; Jiménez-Sanchidrián, C.; Romero-Salguero, F.J.; Esquivel, D. Copper-Complexed Dipyridyl-Pyridazine Functionalized Periodic Mesoporous Organosilica as a Heterogeneous Catalyst for Styrene Epoxidation. *Dalt. Trans.* **2022**, *51*, 4884–4897. [[CrossRef](#)] [[PubMed](#)]
37. Li, S.; Zhou, L.; Su, Y.; Han, B.; Deng, F. ¹³C and ¹⁵N Spectral Editing inside Histidine Imidazole Ring through Solid-State NMR Spectroscopy. *Solid State Nucl. Magn. Reson.* **2013**, *54*, 13–17. [[CrossRef](#)]
38. Bisergaeva, R.; Sirieva, Y. Synthesis of Some Cobaloxime Derivatives. *Earth Environ. Sci.* **2020**, *421*, 072007. [[CrossRef](#)]
39. Markham, L.M.; Mayne, L.C.; Hudson, B.S.; Zgierski, M.Z. Resonance Raman Studies of Imidazole, Imidazolium, and Their Derivatives: The Effect of Deuterium Substitution. *J. Phys. Chem.* **1993**, *97*, 10319–10325. [[CrossRef](#)]
40. Bottari, C.; Rossi, B.; Mele, A.; Damin, A.; Bordiga, S.; Musso, M.; Gessini, A.; Masciovecchio, C. Synchrotron-Based UV Resonance Raman Scattering for Investigating Ionic Liquid-Water Solutions. *Condens. Matter Phys.* **2019**, *22*, 43301. [[CrossRef](#)]
41. Salama, S.; Spiro, T.G. Resonance Raman Spectra of Cobalt(II)-Imidazole Complexes: Analogues of the Binding Site of Cobalt-Substituted Zinc Proteins. *J. Am. Chem. Soc.* **1978**, *100*, 1105–1111. [[CrossRef](#)]
42. Xue, G.; Dai, Q.; Jiang, S. Chemical Reactions of Imidazole with Metallic Silver Studied by the Use of SERS and XPS Techniques. *J. Am. Chem. Soc.* **1988**, *110*, 2393–2395. [[CrossRef](#)]
43. Grzyb, B.; Gryglewicz, S.; Śliwak, A.; Díez, N.; Machnikowski, J.; Gryglewicz, G. Guanidine, Amitrole and Imidazole as Nitrogen Dopants for the Synthesis of N-Graphenes. *RSC Adv.* **2016**, *6*, 15782–15787. [[CrossRef](#)]
44. Chuang, T.J.; Brundle, C.R.; Rice, D.W. Interpretation of the X-Ray Photoemission Spectra of Cobalt Oxides and Cobalt Oxide Surfaces. *Surf. Sci.* **1976**, *59*, 413–429. [[CrossRef](#)]
45. Brown, D.G.; Weser, U. XPS Spectra of Spin-Triplet Cobalt(III) Complexes. *Z. Für Naturforsch. B* **1979**, *34*, 1468–1470. [[CrossRef](#)]
46. Kumar, A.; Pandey, G. A Review on the Factors Affecting the Photocatalytic Degradation of Hazardous Materials. *Mater. Sci. Eng. Int. J.* **2017**, *1*, 106–114. [[CrossRef](#)]
47. Angeles Navarro, M.; Sain, S.; Wünschek, M.; Pichler, C.M.; Romero-Salguero, F.J.; Esquivel, D.; Roy, S. Solar Driven CO₂ Reduction with a Molecularly Engineered Periodic Mesoporous Organosilica Containing Cobalt Phthalocyanine. *Nanoscale* **2023**. [[CrossRef](#)] [[PubMed](#)]

Disclaimer/Publisher’s Note: The statements, opinions and data contained in all publications are solely those of the individual author(s) and contributor(s) and not of MDPI and/or the editor(s). MDPI and/or the editor(s) disclaim responsibility for any injury to people or property resulting from any ideas, methods, instructions or products referred to in the content.